wind

MDPI

Article

Application of a Numerical Simulation to the Estimation of Wind Loads on Photovoltaic Panels Installed Parallel to Sloped Roofs of Residential Houses

Yasushi Uematsu [1,*], Tetsuo Yambe [2] and Atsushi Yamamoto [3]

[1] National Institute of Technology (KOSEN), Akita College, Akita 011-8511, Japan
[2] Tohoku Electric Power Network Corporation, Sendai 980-8551, Japan; yambe.tetsuo.wh@tohoku-epco.co.jp
[3] Asahi Kasei Homes Corporation, Tokyo 101-8101, Japan; yamamoto.ar@om.asahi-kasei.co.jp
* Correspondence: uematsu@akita-nct.ac.jp; Tel.: +81-18-847-6001

Abstract: Many residential houses with sloped roofs are equipped with photovoltaic (PV) systems. In Japan, PV systems are generally designed based on JIS C 8955, which specifies wind force coefficients for designing PV panels. However, no specification is provided to the PV panels installed near the roof edges where high suctions are induced. When installing PV panels in such high-suction zones, we need to evaluate the wind loads on the PV panels appropriately, usually by performing a wind tunnel experiment. However, it is difficult to make wind tunnel models of PV panels with the same geometric scale as that for the building, e.g., 1/100, because the thickness of PV panels and the distance between PV panels and a roof are both several centimeters. Therefore, in the present paper a numerical simulation is applied to the estimation of pressures in the space between the lower surface of PV panels and the roof surface, called "layer pressures", using the unsteady Bernoulli equation and the time histories of external pressure coefficients obtained from a wind tunnel experiment. An assumption of the weak compressibility of the air and an adiabatic condition is made for predicting the layer pressures from the flow speed through the gaps. The simulation method is validated by a wind tunnel experiment using a model of square-roof building.

Keywords: photovoltaic panel; wind load; sloped roof; wind tunnel experiment; numerical simulation; unsteady Bernoulli equation

check for updates

Citation: Uematsu, Y.; Yambe, T.; Yamamoto, A. Application of a Numerical Simulation to the Estimation of Wind Loads on Photovoltaic Panels Installed Parallel to Sloped Roofs of Residential Houses. *Wind* **2022**, 2, 129–149. https://doi.org/10.3390/wind2010008

Academic Editor: Charalampos Baniotopoulos

Received: 27 December 2021
Accepted: 24 February 2022
Published: 3 March 2022

Publisher's Note: MDPI stays neutral with regard to jurisdictional claims in published maps and institutional affiliations.

Copyright: © 2022 by the authors. Licensee MDPI, Basel, Switzerland. This article is an open access article distributed under the terms and conditions of the Creative Commons Attribution (CC BY) license (https://creativecommons.org/licenses/by/4.0/).

1. Introduction

The objective of the present paper is to investigate the application of a numerical simulation based on the unsteady Bernoulli equation to the estimation of wind loads on PV panels installed parallel to sloped roofs of residential houses. Special attention is paid to a square roof. In the simulation, the time histories of external pressure coefficients on the roof, obtained from a wind tunnel experiment, were employed.

Power generation by photovoltaic (PV) systems has become popular worldwide due to the consideration for environmental conservation. In Japan, it is effective to install PV panels at a tilt angle of 20° to 40° with respect to the horizontal plane considering the power generation efficiency. Sloped roofs with a pitch of 20° to 40° are often used for residential houses in Japan. Therefore, PV panels installed parallel to the sloped roofs are very effective. However, being vulnerable to dynamic wind actions, they are often subjected to damage or collapse due to strong winds, such as those by typhoons and downbursts [1].

For reducing wind damage to PV systems, it is necessary to estimate the wind loads on PV panels accurately and to evaluate the wind resistant performance of PV systems appropriately. Many researchers have experimentally and/or numerically investigated the wind loads on tilted PV panels installed on the ground [2–9] or on flat roofs of large commercial buildings [10–21]. By comparison, only a few investigations have been made of the wind loads on PV panels installed parallel to sloped roofs of residential houses [22–26].

Geurts and Blackmore [22] performed full-scale and wind tunnel experiments to investigate the net uplift loads acting on a stand-off PV system installed parallel to the roof of an existing house with a roof pitch of $\beta = 42^\circ$. In the full-scale measurements, two dummy PV panels (1.6 m long, 0.8 m wide and 18 mm thick) were mounted on the roof. The distance H_{panel} between the panel's lower surface and the roof surface was about 150 mm. The geometric scale of the wind-tunnel model was 1/100. The value of H_{panel} was changed from 0.25 mm to 3 mm (from 25 mm to 300 mm at full scale). The results indicated that the net wind loads on the PV panels were substantially lower than the external loads on the roof surface. Furthermore, it was found that the effect of H_{panel} on the net wind loads was relatively small. This feature may be related to such a high roof pitch as $\beta = 42^\circ$. Aly and Bitsuamlak [23] measured the wind forces on PV panels installed on gable roofs with two distinct pitches—i.e., 14° and 22.6°—in a wind tunnel. The geometric scale of the models was 1/15. The value of H_{panel} was fixed to 0.1524 m at full scale. They tested three kinds of panel dimensions (small: 0.9144 m × 1.524 m, medium: 1.524 m × 2.4384 m, and big: 1.524 m × 2.7432 m) and four kinds of panel arrangements; the PV panels were installed almost all over the roof. Focus was on the effects of panel dimension and arrangement on the net wind loads of PV panels. Results indicated that the cladding loads on individual panel were smaller or larger in magnitude than those on the corresponding area of a bare roof (roof without PV panels), depending on the location and dimension of panels, as well as on the roof pitch β. Panels located close to the roof corners and edges were generally subjected to lower net pressures than the external pressures on the bare roof. Aly and Bitsuamlak recommended to avoid mounting PV panels in these zones, because the PV panels would be subjected to high suctions. Stenabough et al. [24] made a similar wind tunnel experiment using a gable roof model with $\beta = 30^\circ$. The geometric scale of the model was 1/20. The PV panels were modeled by flat panels with equivalent full-scale dimensions of 50 cm width, 145.5 cm length and 6 cm thickness. Focus was on the effects of the horizontal gap G between PV panels and H_{panel} on the area-averaged wind loads of PV panels. It was found that larger G values and smaller H_{panel} values yielded lower net wind loads due to pressure equalization, which resulted in the magnitude of net wind loads typically being lower than those for the bare roof surface. Naeiji et al. [25] investigated the net wind loads of PV panels installed on flat, gable and hip roofs using large models in a large wind tunnel, the cross-section of which is 6 m wide and 4 m high. To the authors' best knowledge, only this study dealt with a hip roof. The geometric scale of the models was 1/6. The panel was 2 m long, 1 m wide and 0.15 m thick at full scale. An investigation was conducted on the effects of building height H, panel clearance distance H_{panel} and panel tilt angle β_{panel} on the area-averaged wind loads of PV panels. Note that β_{panel} was not necessarily equal to the roof pitch β. The value of H_{panel} was either 0.3 m or 0.45 m at full scale, which is much larger than that of practical PV systems generally used in Japan. The results indicated that the critical wind direction generating the worst maximum or minimum peak wind force coefficient depended on the roof shape as well as on β_{panel}.

Takamori et al. [26] conducted a wind tunnel experiment on the wind loads of PV panels installed parallel to gable roofs of low-rise buildings. The geometric scale of the models was 1/30. There was no horizontal gap between PV panels, i.e., $G = 0$ m. The PV panels were 1.06 m long and 0.86 m wide at full scale. The thickness of panel models was 3 mm (90 mm at full scale). The panels were not installed in the edge zones up to 0.3 m at full scale from the roof edges (eaves, gable and ridge). The values of β and H_{panel} were changed from 10° to 40° and from 30 mm to 150 mm at full scale, respectively. Based on the results, they proposed positive and negative wind force coefficients for designing PV panels. It was noted that the magnitude of negative wind force coefficients might become larger than that of the proposed values when $H_{\text{panel}} > 100$ mm.

Hip roofs are widely used for residential houses in Japan. Recently, PV panels are often installed parallel to these roofs, as shown in Figure 1. Such PV systems are generally designed based on JIS (Japanese Industrial Standard) C 8955 [27], which is based on the experimental results of Takamori et al. [26]. This standard provides wind force coefficients

for designing PV panels installed on building's roofs. However, no specification is provided to PV panels located near the roof edges, up to 0.3 m from the edge. It is not recommended to install PV panels in such zones, because large up-lift forces are generated on the PV panels by flow separation at the roof edges [28,29]. When installing PV panels in such high-suction zones, we need to estimate the wind loads on the PV panels accurately. For estimating wind loads on structures we usually make a wind tunnel experiment. However, it is quite difficult to make wind tunnel models of PV panels with the same geometric scale as that of the building, such as 1/100, for example. The thickness t_{PV} and the distance D_{cavity} between the lower surface of PV panels and the roof surface are both as small as several centimeters. When the geometric scale of the wind tunnel model is 1/100, the values of t_{PV} and D_{cavity} should be less than 1 mm, such as 0.6 mm, for example. Furthermore, we have to measure the pressures on both the upper and lower surfaces of PV panels simultaneously for evaluating the net wind pressures (wind forces) on PV panels, which also makes it difficult to make wind tunnel models of PV panels. Indeed, some deformed models of PV panels are often used in wind tunnel experiments [26].



Figure 1. PV panels installed parallel to the hip roof of a residential building.

In the present paper, we apply a numerical simulation based on the unsteady Bernoulli equation to the estimation of wind pressures on the lower surface of PV panels installed parallel to sloped roofs of residential houses. The pressure in the space between the lower surface of PV panels and the roof surface is called "layer pressure" in the present paper. The layer pressure acts on the lower surface of PV panel as well as on the roof surface. In the numerical simulation we use the time histories of external pressure coefficients simultaneously measured at many points on the roof in a turbulent boundary layer (wind tunnel experiment). Among many kinds of sloped roofs, focus is on a square roof with no projection of eaves, because it is the simplest configuration of sloped roof. Two types of panel arrangements are tested. That is, PV panels are arranged with no gap between them (G = 0 m) in one case and with a small gap between them along the short sides in the other case. The simulation method for evaluating the layer pressures is validated by a wind tunnel experiment, in which some modifications are made on the model of PV panels, as was done in previous studies [26]. Note that the main purpose of this paper is not to provide the wind force coefficients for designing PV systems but to investigate the application of the numerical simulation to the estimation of layer pressures. Similar simulations have been applied to the wind-load estimations of air-permeable double-layer roof systems, loose-laid roof-insulation systems, roofing tiles, permeable unit flooring decks and others [30–35]. To the authors' best knowledge, no previous studies have applied such a numerical simulation to the wind load estimation of PV panels installed parallel to sloped roofs of low-rise buildings.

The present paper consists of four sections. Section 2 describes the wind tunnel experiment for measuring the external pressures on the roof and PV panels. Two kinds of building models are used; one has no PV panels and the other has PV panels installed parallel to the roof. The characteristics of pressure distributions on the roof and PV panels

are described. The wind pressure distribution on the PV panels is compared with that on the bare roof in order to investigate the effect of PV panels on the flow field around the roof. It is found that the pressure distribution on the PV panels is similar to that on the bare roof. Therefore, the time histories of wind pressure coefficients on the bare roof are used for the numerical simulation of the layer pressures in the following section. This is also because it is difficult to make models of PV panels with the same geometric scale as that for the building, as mentioned above. Brief discussion is made of the wind forces on the PV panels as well as on the roof. Then, Section 3 investigates the application of a numerical simulation based on the unsteady Bernoulli equation to the evaluation of layer pressures. First, the simulation method is briefly explained. Then, the simulation results for the wind loads on PV panels are compared with the experimental ones in order to validate the simulation method. The effect of PV panels on the wind pressures on the roof is also discussed. Finally, Section 4 summarizes the conclusions obtained from the present study

2. Wind Tunnel Experiment

2.1. Wind Tunnel Model

The present study focuses on the PV panels installed parallel to the roof of a square-roof building, as shown in Figure 2. The width, depth and eaves height of the building are 11 m, 11 m and 8.2 m, respectively. The roof pitch is 25°, which is often used for residential houses in Japan. Consequently, the roof top is 10.7 m high. The roof has no overhang. Three kinds of wind tunnel models, as shown in Figure 3, are used in the experiment. The models are made with a geometric scale of $\lambda_L = 1/75$ using acrylic plates of 2 mm thickness. These models are named A, B0 and B1, respectively. Model A is not equipped with PV panels on the roof. Model B0 and B1 are equipped with PV panels almost all over a roof surface; the difference between Models B0 and B1 will be described later. The PV panels are also modeled by 2 mm thick acrylic plate. Therefore, the model is somewhat thicker than the practical ones considering that the geometric scale of the model is $\lambda_L = 1/75$. However, this is a limitation in making models of PV panels. Similar modified models of PV panels were used in previous studies [26].

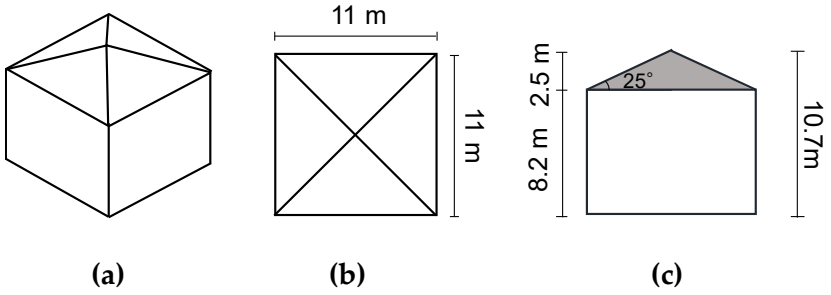

Figure 2. Square-roof building considered in the present study: (**a**) General view; (**b**) Plan; (**c**) Elevation.

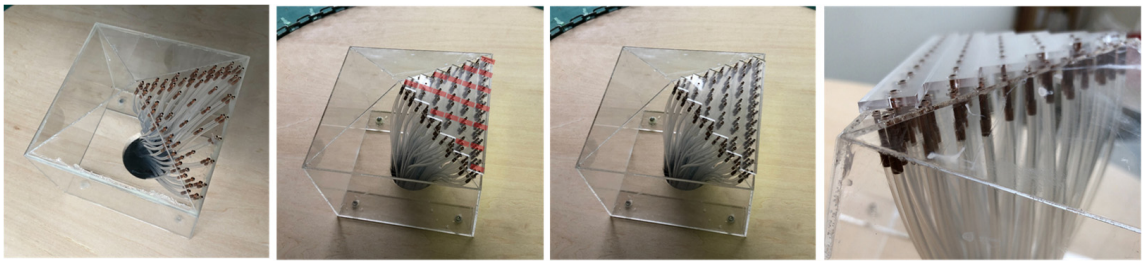

Figure 3. Wind tunnel models: (**a**) Model A; (**b**) Model B0; (**c**) Model B1; (**d**) Close-up view of the installed PV panels.

Figure 4 shows the details of the model of PV panels for Model B1. The distance between the roof surface and the lower surface of PV panels is 1 mm. The PV panels are generally installed on horizontal rails mounted on pedestals, as shown in Figure 5. The horizontal rails are modeled by ribs 0.5 mm wide and 0.5 mm high. The pedestals are not reproduced in the model, because they may minutely affect the cavity flow under PV panels. It is assumed that the PV panels are arranged with gaps between them along the short sides. The gap width is tentatively assumed 10 mm at full scale in the present study. The net wind pressure (wind force) on PV panel is provided by the difference between the pressures on the upper and lower surfaces of the panel; the magnitude of net wind pressures may be reduced by pressure equalization due to the gaps [24]. Because the gap of 10 mm width cannot be reproduced as it is with a geometric scale of $\lambda_L = 1/75$, it is replaced by a circular hole of 1 mm diameter, the area of which is almost equal to that of the gap. The circular hole is placed at the center of gap (see Figure 6). In Model B0, PV panels are arranged with no gap between them; that is, the PV panels are in contact with each other. In practice, Model B0 is obtained by covering the circular holes drilled on the PV panel model of Model B1 with thin adhesive tape.

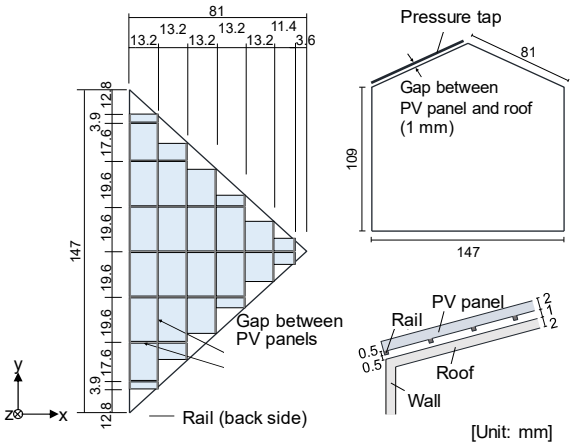

Figure 4. Arrangement and size of PV panels.

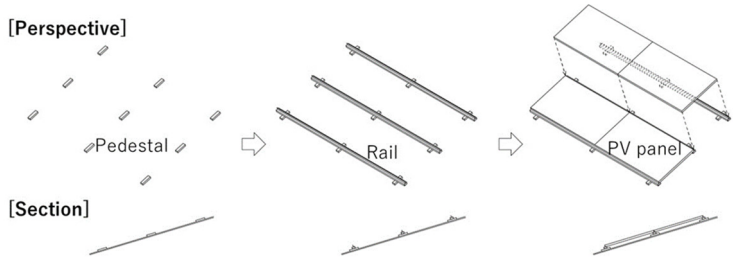

Figure 5. Schematic illustration of PV panel installation method.

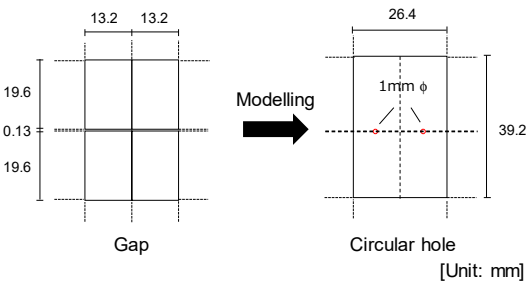

Figure 6. Modelling of gaps between PV panels.

Figure 7 shows the location of pressure taps (diameter φ = 0.6 mm) installed on the roof and on the upper surface of PV panels. Because high suctions are induced near the roof edges, many pressure taps are arranged in the edge zones. Pressure taps are not installed on the lower surface of PV panels. Because the distance between the lower surface of PV panels and the roof surface is small, the pressure on the lower surface of PV panel can be replaced by that on the roof at the same location [23]. The model of PV panels is supported by brass pipes of 1 mm outer diameter connecting to the pressure taps, as shown in Figure 3d. The effect of the brass tubes on the cavity flow under PV panels can be neglected, because the outer diameter of brass pipes is as small as 1 mm and the cavity flow is regarded as a laminar flow [35,36].

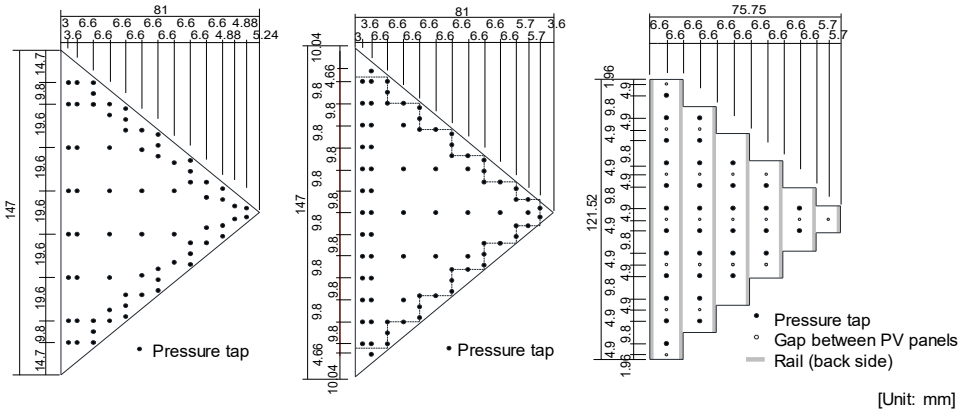

Figure 7. Arrangement of pressure taps on the roof and PV panels: (**a**) Roof (Model A); (**b**) Roof (Model B0, B1); (**c**) PV panel (Model B0, B1).

2.2. Wind Tunnel Flow

The experiment is conducted in an Eifel type wind tunnel at the Department of Architecture and Building Science, Tohoku University, which has a working section 1.4 m wide, 1.0 m high and 6.5 m long. The wind tunnel flow is a turbulent boundary layer. The profiles of mean wind speed U_z and turbulence intensity I_z at the location of the model's center without model are plotted in Figure 8a. The power-law exponent α for the mean wind speed profile is about 0.27 and the turbulence intensity I_H at the mean roof height H (=0.126 m) is about 0.17. Figure 8b shows the normalized power spectral density function, $fS_u(f)/{\sigma_u}^2$, of fluctuating wind speed at a height of z = 100 mm, where $S_u(f)$ = power spectral density function, f = frequency, σ_u = standard deviation of fluctuating wind speed, and L_x = integral length scale of turbulence. It is found that the general shape of $S_u(f)$ agrees well with that of the Karman-type spectrum with L_x = 0.2 m (solid line in Figure 8b). According to the AIJ *Recommendations for Loads on Buildings* [37], the values of α, I_H and L_x for Terrain Category III (typical of suburban exposure) are specified as 0.20, 0.26 and 58 m at full scale, respectively. Comparing the above-mentioned values of the wind tunnel flow with these specified values, we can find that α is larger, while I_H and L_x are smaller. In particular, the value of L_x is as small as about 1/4 of the target value, considering that the geometric scale is 1/75. In wind tunnel experiments for low-rise buildings, it is generally difficult to satisfy the similarity for all of these parameters, particularly for L_x. Tieleman et al. [38–40] investigated the effects of these parameters on the characteristics of wind pressures on the roofs of low-rise buildings. They found that the fluctuating wind pressures were minutely affected by α. By comparison, the effect of I_H was significant. Furthermore, the fluctuating pressures were less sensitive to L_x. Regarding the effect of L_x on the roof pressures they mentioned that the wind tunnel experiment could reproduce the fluctuating wind pressures almost satisfactorily, provided that the L_x value of the wind tunnel flow was larger than 0.2 times the target value and the maximum length of the wind

tunnel model. The wind tunnel flow used in this study satisfies this criterion. That is, the value of L_x (≈0.2 m) of the wind tunnel flow is larger than 0.2 times the target value (=58 m/75 = 0.77 m) and the largest size of the building (=10.7/75 = 0.14 m). Tieleman [39] also found that a small-scale turbulence parameter S defined by Equation (1) played an important role on the flow simulation in wind tunnel experiments for low-rise buildings:

$$S = \frac{f_s S_u(f_s)}{{\sigma_u}^2} \left(\frac{\sigma_u}{U}\right)^2 \times 10^6,\ f_s = \frac{10U}{L_B} \tag{1}$$

where U = mean wind speed, and L_B = characteristic length of the building. The wind pressure fluctuations were sensitive to S up to about 300, but they were minutely affected by S when $S > 300$. Therefore, the value of S should be larger than about 300. The value of S of the wind tunnel flow used in the present study was about 470, which was larger than 300. Note that U_H and H are used for U and L_B in Equation (1). Although the I_H value of the wind tunnel flow is somewhat smaller than the target value, such a disagreement can be acceptable, because the main purpose of the present study is not to estimate the design wind loads on PV panels precisely but to investigate the application of the numerical simulation to the wind load estimation of PV panels.

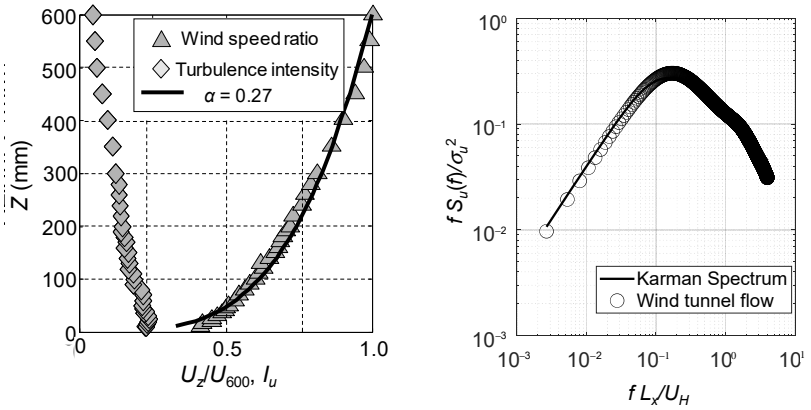

(**a**) (**b**)

Figure 8. Characteristics of wind tunnel flow at the location of model's center without model: (**a**) Profiles of mean wind speed and turbulence intensity; (**b**) Normalized power spectral density function.

2.3. Experimental Procedure

The design wind speed U_H at the mean roof height H (=9.45 m) is calculated based on the AIJ *Recommendations for Loads on Buildings* [37]. The '*Basic wind speed*' U_0 is set to 35 m/s as a representative value for the Main Island of Japan. The terrain category is assumed to be III. In practice, U_H is calculated as 27.8 m/s. The value of U_H of the wind tunnel flow is set to 8 m/s. The Reynolds number Re, defined in terms of U_H and H, is approximately 6.7×10^4. The blockage ratio Br of the model with respect to the wind tunnel's cross-section is about 1.9% at a maximum. The values of Re and Br satisfy the experimental criteria recommended in *Wind Tunnel Testing for Buildings and other Structures* [41]; that is, $Re > 1.1 \times 10^4$ and $Br < 5\%$. The velocity scale λ_V is approximately 1/3.5. Considering that the geometric scale is $\lambda_L = 1/75$, the time scale λ_T ($=\lambda_L/\lambda_V$) is calculated as approximately 1/22.

The wind direction θ, defined as shown in Figure 9, is varied from 0° to 180° at an increment of 15°, considering the symmetry of the model. The pressure taps are connected to pressure transduces (Wind Engineering Institute, MAPS-02, Midview City, Singapore) via brass pipes of 0.6 mm ID and flexible vinyl tubes of 1 mm ID. The total length of the tubing is 1 m. The sampling rate of pressure measurements is 800 Hz. The sampling time is 10 min at full scale (approximately 28 s at model scale). A low-pass filter with a

cut-off frequency of 300 Hz is used to remove high-frequency noise from the signals. The measurements are repeated 10 times under the same condition.

The wind pressure coefficient C_p is defined by

$$C_p = \frac{P - P_s}{q_H} \tag{2}$$

where P = pressure on the structure; P_s = static pressure in the wind tunnel; and q_H = mean velocity pressure ($=\frac{1}{2}\rho U_H{}^2$, with ρ being the air density) of approach flow at the mean roof height H. The wind force (net wind pressure) acting on PV panel is provided by the difference between the pressures, P_t and P_b, on the upper and lower surfaces. The lower surface pressure P_b is equal to the layer pressure P_l under the PV panel. Therefore, the wind force coefficient, or the net wind pressure coefficient, C_f, is provided by the following equation:

$$C_f = \frac{P_t - P_b}{q_H} \approx \frac{P_t - P_l}{q_H} = \frac{P_t - P_s}{q_H} - \frac{P_l - P_s}{q_H} = C_{pt} - C_{pl} \tag{3}$$

where C_{pt} represents the wind pressure coefficient on the upper surface of PV panel; and C_{pl} is called "layer pressure coefficient" in this paper. When evaluating the statistical values of wind pressure and force coefficients, we apply ensemble averaging to the results of the 10 measurements conducted under the same condition. The distortion of measured fluctuating pressures due to tubing is compensated by using the frequency response function of the measuring system in the frequency domain. No moving average is applied to the time histories of wind pressure and force coefficients.

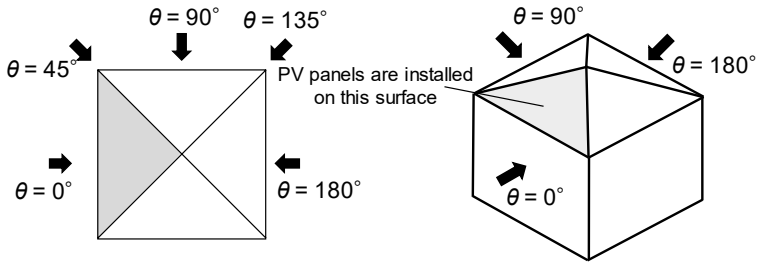

Figure 9. Definition of wind direction.

2.4. Experimental Results

2.4.1. Wind Pressures on the Roof without PV Panels

First, the characteristics of wind pressures on the square roof are investigated based on the results for Model A. Figures 10 and 11 respectively show the distributions of the maximum and minimum peak pressure coefficients, $\hat{C}_{pe}$ and $\check{C}_{pe}$, on the roof when $\theta = 0°$ and 45°. Note that $\hat{C}_{pe}$ and $\check{C}_{pe}$ refer to the maximum and minimum peak values of wind pressure coefficients C_{pe} during a period of 10 min at full scale, which can be obtained from the time history of C_{pe}. Large positive pressures occur near the windward eaves at both wind directions. However, the magnitude is not so large. On the other hand, large suctions occur near the windward eaves when $\theta = 0°$ and near the ridge when $\theta = 45°$. These suctions are induced by flow separation at the windward eaves or ridge. Figure 12a,b, respectively show the distributions of the most critical maximum and minimum peak pressure coefficients, $\hat{C}_{pe,\mathrm{cr}}$ and $\check{C}_{pe,\mathrm{cr}}$ irrespective of wind direction, i.e., the maximum value of $\hat{C}_{pe}$ and the minimum value of $\check{C}_{pe}$ among all wind directions. The maximum value of $\hat{C}_{pe,\mathrm{cr}}$ among all pressure taps is 0.66 when $\theta = 45°$ and the minimum value of $\check{C}_{pe,\mathrm{cr}}$ among all pressure taps is -4.1 when $\theta = 0°$. These values occur at pressure taps marked by white circles in Figures 10b and 11a. The present results for the wind pressure distributions on the square roof are consistent with those of previous studies investigating the wind pressure distributions on hip roofs [42–48].

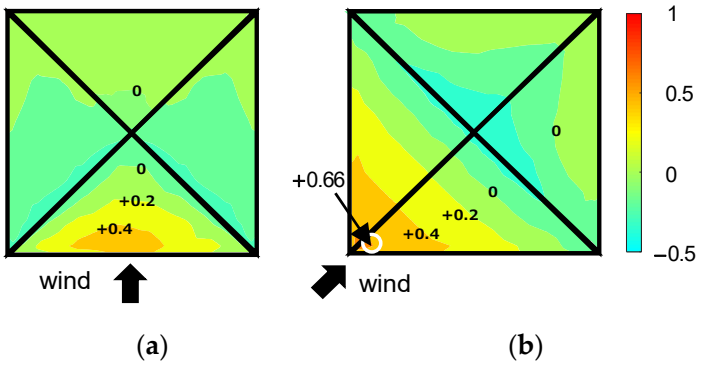

Figure 10. Distribution of the maximum peak pressure coefficients $\hat{C}_{pe}$ on the roof (Model A): (**a**) $\theta = 0°$; (**b**) $\theta = 45°$.

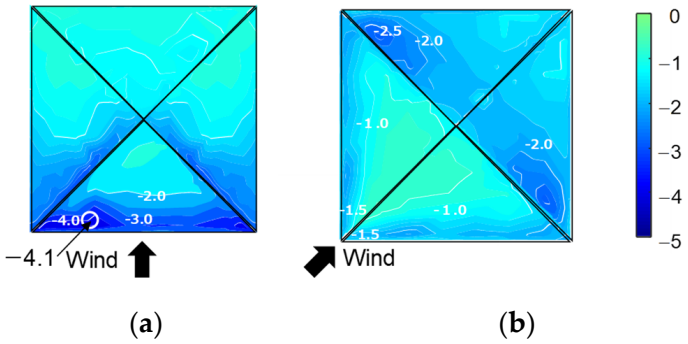

Figure 11. Distribution of the minimum peak pressure coefficients $\check{C}_{pe}$ on the roof (Model A): (**a**) $\theta = 0°$; (**b**) $\theta = 45°$.

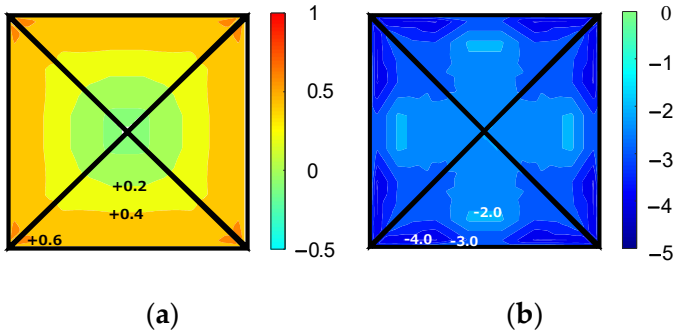

Figure 12. Distributions of the most critical maximum and minimum peak pressure coefficients, $\hat{C}_{pe,\mathrm{cr}}$ and $\check{C}_{pe,\mathrm{cr}}$, irrespective of wind direction on the roof (Model A): (**a**) $\hat{C}_{pe,\mathrm{cr}}$; (**b**) $\check{C}_{pe,\mathrm{cr}}$.

2.4.2. Wind Pressures and Forces on PV Panels

Figure 13 shows the distributions of the minimum peak pressure coefficients, $\check{C}_{pe}$ and $\check{C}_{pt}$, on the roof of Model A and on the PV panels (upper surface) of Model B0 when $\theta = 0°$, 45° and 90°. It is found that the distributions of $\check{C}_{pe}$ and $\check{C}_{pt}$ are similar to each other. Figures 14 and 15, respectively, show the maximum and minimum peak pressure coefficients among all pressure taps on the roof of Model A and on the PV panels (upper surface) of Model B0 at each wind direction θ. Regarding the maximum peak pressure coefficients, both results agree well with each other. Regarding the minimum peak pressure coefficients, on the other hand, the results for Model B0 are somewhat smaller in magnitude than those for Model A in oblique winds. Similar behavior can be observed in the results for θ = 75–90°. This feature may be due to a small change in the characteristics of flow separation at the ridge or windward eaves by installing PV panels on the roof. That is, a change in the roof configuration by installing PV panels affects the separated flow, resulting

in a change in the pressure distribution on the roof or on the PV panels. However, the effect is not so significant; the maximum difference is about 0.4. Considering that practical PV panels are thinner than the present model at full scale, it is thought that PV panels affect the flow around the roof only slightly. In other words, we can predict the values of layer pressures under PV panels based on the wind pressure coefficients on the roof obtained from a wind tunnel experiment using a building model without PV panels.

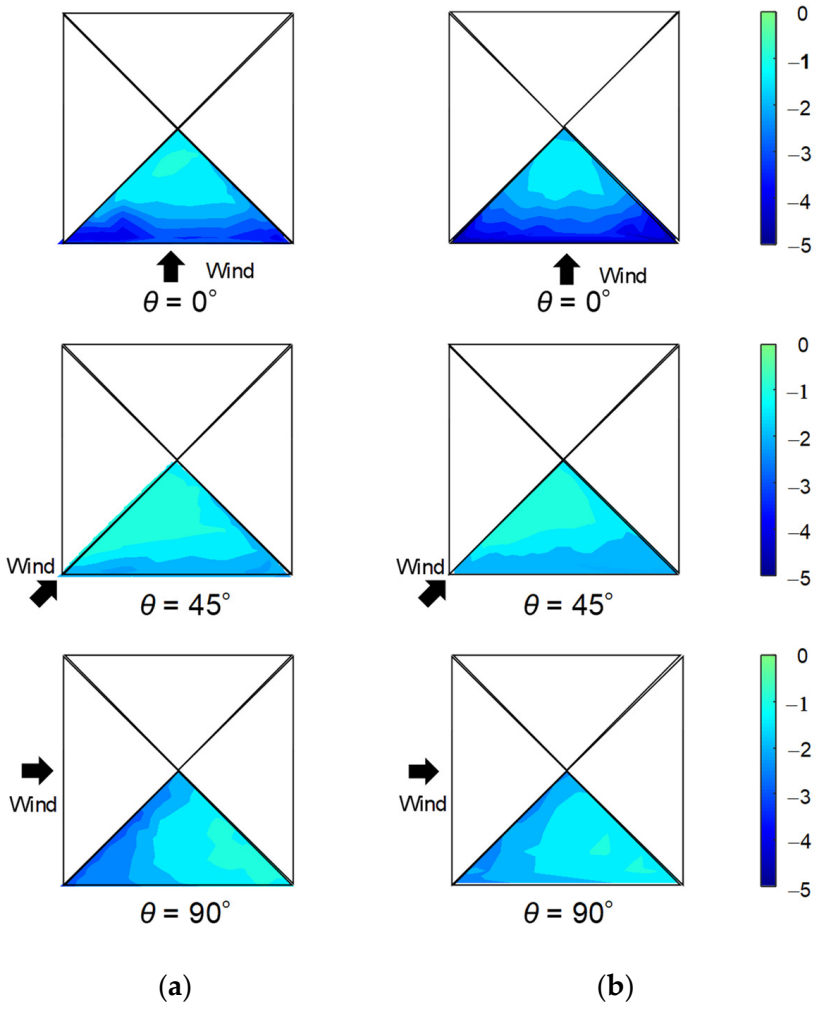

Figure 13. Distributions of the minimum peak pressure coefficients when θ = 0°, 45° and 90°: (**a**) Model A; (**b**) Model B0.

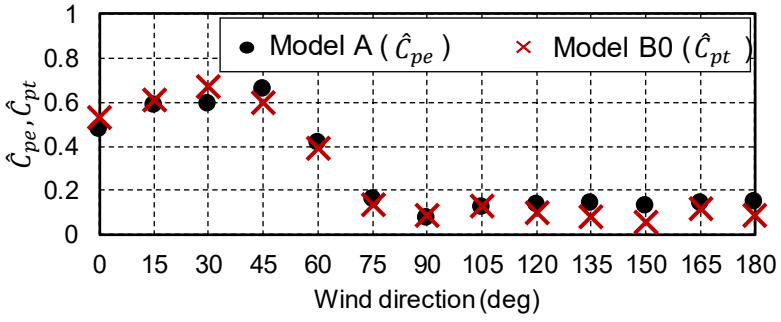

Figure 14. Maximum peak pressure coefficient among all pressure taps at each wind direction.

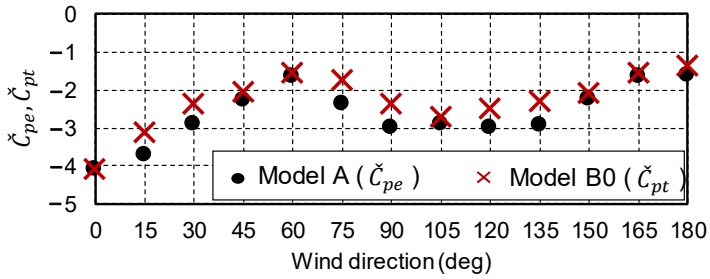

Figure 15. Minimum peak pressure coefficient among all pressure taps at each wind direction.

In the present model, 26 rectangular PV panels are installed on the roof; the definition of panel numbers is shown in Figure 16. The PV panels labelled by red figures are subjected to large up-lift forces, as will be described later (see Table 1). Area-averaged wind force coefficient $C_{f,\text{area}}$ is calculated for each PV panel. Because the resolution of pressure taps on the wind tunnel model is relatively coarse, we apply the cubic spline function to the experimental data of C_f in order to obtain the C_f values at the lattice points of a fine grid, from which the value of $C_{f,\text{area}}$ is computed for each panel. Then, the maximum and minimum peak area-averaged wind force coefficients, $\hat{C}_{f,\text{area}}$ and $\check{C}_{f,\text{area}}$, are obtained from the time history of $C_{f,\text{area}}$ for each PV panel. Figure 17 shows the minimum value of $\check{C}_{f,\text{area}}$ among all panels at each wind direction, in which the results for Models B0 and B1 are plotted in order to investigate the effect of gaps between panels on $\check{C}_{f,\text{area}}$. Table 1 shows the PV panel that provides the minimum value of $\check{C}_{f,\text{area}}$ among all panels at each wind direction. Note that the same wind direction provides the minimum values for both Models B0 and B1. It can be seen that the results for Models B0 and B1 show a similar trend. The minimum values occurred on panels located near the eaves or ridge. In particular, panels located near the windward eaves exhibited large-magnitude negative values (upward) when θ = 0–30°. The largest one was −3.7 for Model B0 and −3.3 for Model B1, which occurred on Panel 4 at θ = 0°. It is found that the values for Model B1 are generally smaller in magnitude than those for Model B0. The largest difference between these two models is about 0.4 at θ = 0°. This feature may be due to the pressure equalization caused by the gaps between PV panels, as Stenabough et al. [24] indicated.

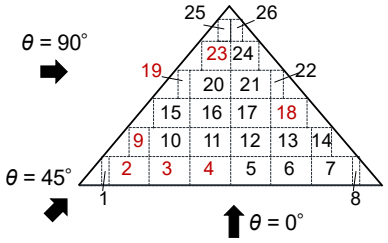

Figure 16. Definition of PV panel numbers.

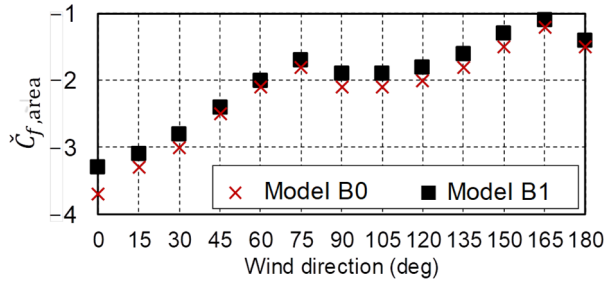

Figure 17. Minimum peak value of area-averaged wind force coefficient among all panels at each wind direction.

Table 1. PV panel number that provides the minimum peak area-averaged wind force coefficient at each wind direction.

θ (deg)	0	15	30	45	60	75	90	105	120	135	150	165	180
Panel	4	3	2	3	3	23	9	23	19	19	9	19	18

The most critical maximum and minimum peak area-averaged wind force coefficients irrespective of wind direction, $\hat{C}_{f,\mathrm{area,cr}}$ and $\check{C}_{f,\mathrm{area,cr}}$, in the edge and internal zones of Model B0 are compared with the specified values by JIS C 8955 [27] in Table 2. It should be mentioned that the Standard does not specify the wind force coefficients for PV panels located in the edge zone up to 30 cm from the edge; therefore, a direct comparison cannot be made for the edge zone in a strict sense. Furthermore, the Standard specifies the positive and negative wind force coefficients, $C_{f,\mathrm{positive}}$ and $C_{f,\mathrm{negative}}$, and the gust effect factor G_f. The values of $G_f \times C_{f,\mathrm{positive}}$ and $G_f \times C_{f,\mathrm{negative}}$, respectively, correspond to $\hat{C}_{f,\mathrm{area,cr}}$ and $\check{C}_{f,\mathrm{area,cr}}$, obtained from the present wind tunnel experiment. The values of $\hat{C}_{f,\mathrm{area,cr}}$ and $\check{C}_{f,\mathrm{area,cr}}$ predicted from the C_{pe} distributions on the roof of Model A are also presented in Table 2 for a comparative purpose. In the computation we assume that the net wind force on a PV panel is equal to that on the corresponding area of Model A (bare roof). The results indicate that the Standard provides conservative values of wind force coefficient for the panels in the internal zone. As might be expected, the value of $\check{C}_{f,\mathrm{area,cr}}$ for the panels in the edge zone is larger in magnitude than that in the internal zone. The value of $\check{C}_{f,\mathrm{area,cr}}$ for the panels in the edge zone predicted from the C_{pe} distribution on the roof of Model A is somewhat larger in magnitude than those obtained from the direct measurements. Considering that the negative (up-lift) wind forces dictate the structural design of PV panels in practice, we can conclude that the design wind loads on PV panels can be estimated from the wind pressure coefficient distribution on the bare roof on the safer side.

Table 2. The most critical positive and negative peak wind force coefficients irrespective of wind direction for panels in the edge and internal zones, compared with the specification of JIS C 9855 [27].

Data Source	Positive Value		Negative Value	
	Edge Zone	**Internal Zone**	**Edge Zone**	**Internal Zone**
JIS C 8955 ($G_f \times C_{f,\mathrm{positive}}$, $G_f \times C_{f,\mathrm{negative}}$)	–	+2.85	–	−2.81
Experiment & simulation ($\hat{C}_{f,\mathrm{area,cr}}$, $\check{C}_{f,\mathrm{area,cr}}$)	+2.34	+1.84	−3.70	−2.58
Prediction from the C_p distribution	+1.79	+1.65	−4.18	−2.62

2.4.3. Effect of PV Panels on the Roof Pressures

Figure 18 shows the distributions of the minimum peak pressure coefficients on the roof of Model B0 for some typical wind directions ($\theta = 0^\circ$, 45° and 90°) and for all wind directions. As might be expected, the magnitude is small in the internal zone, while it is large near the ridges. It can be found that the distributions are quite different from those for Model A (see Figures 12b and 13). Furthermore, the magnitude of the minimum peak pressure coefficients is found to be reduced significantly by installing PV panels.

Figure 19 shows the minimum peak pressure coefficient among all pressure taps on the roof of Model A at each wind direction, compared with that of Model B1. We can see a significant reduction of the magnitude of suctions on the roof by installing PV panels on the roof when $\theta = 0^\circ$, 15°, 105° and 120°. In particular, the effect is very large when $\theta = 0^\circ$.

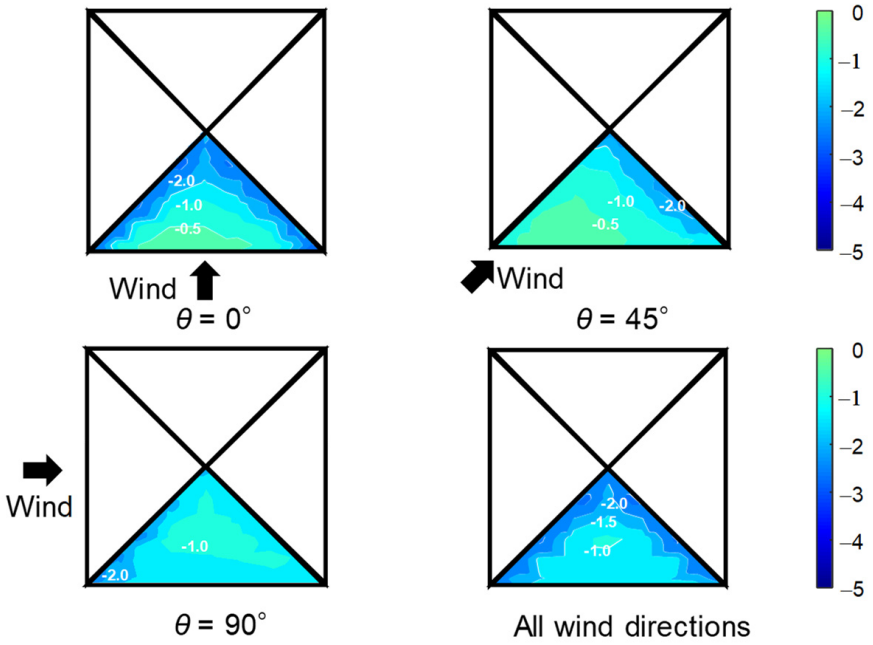

Figure 18. Distributions of the minimum peak pressure coefficients on the roof (Model B0).

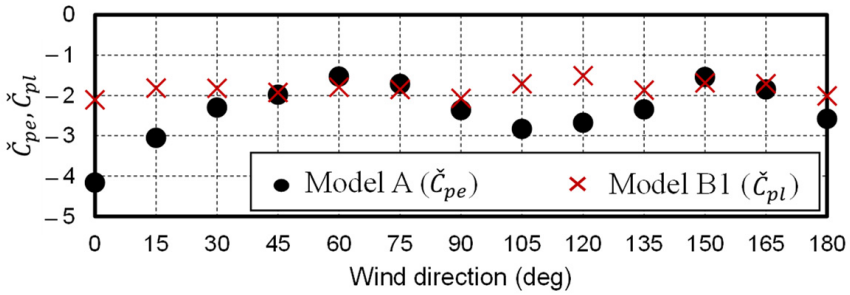

Figure 19. Minimum peak pressure coefficients among all pressure taps on the roof at each wind direction.

3. Numerical Simulation of Layer Pressures

3.1. Method of Simulation

The method of simulation used in the present paper is the same as that we employed in our previous paper [49], in which we applied this method to the evaluation of wind loads on PV panels horizontally installed on flat roofs. The original idea of this method came from Amano et al. [30], Okada et al. [31] and Oh and Kopp [32]. In the simulation, we estimate the layer pressures using the unsteady Bernoulli equation and the time histories of the external wind pressure coefficients at the gap location, which were obtained from the above-mentioned wind tunnel experiment. The method is briefly explained here; regarding the details, see Uematsu et al. [49].

The space under PV panels is divided into many sub-spaces called "Rooms" [33], as shown in Figure 20. Note that the subject is similar to the problem of building internal pressures, when the space under PV panels is regarded as a building [30]. The pressure in each Room is a function of time but assumed spatial uniformity. The unsteady Bernoulli equation is applied to the cavity flows between Rooms, as well as to the gap flows between the external space and Rooms. The driving forces of the gap and cavity flows are the pressure differences between Rooms or between the external space and Room. The governing

equations for the gap and cavity flows in the x, y and z directions (regarding the coordinate, see Figure 4) may be given by the following equations (see [49]):

$$\frac{\rho l_{i,j}\dot{U}_{i,j+1}}{q_H} = C_{i,j} - C_{i,j+1} - \frac{1}{2q_H}C_L\rho_{i,j}U_{i,j+1}\left|{}_{i,j}U_{i,j+1}\right| - \frac{\Delta p_x}{q_H} \tag{4}$$

$$\frac{\rho l_{i,j}\dot{U}_{i+1,j}}{q_H} = C_{i,j} - C_{i+1,j} - \frac{1}{2q_H}C_L\rho_{i,j}U_{i+1,j}\left|{}_{i,j}U_{i+1,j}\right| - \frac{\Delta p_y}{q_H} \tag{5}$$

$$\frac{\rho l_e\dot{U}_{i,j}}{q_H} = C_{i,j} - {}_eC_{i,j} - \frac{1}{2q_H}C_{Le}\rho_e U_{i,j}\left|{}_eU_{i,j}\right| - \frac{\Delta p_e}{q_H} \tag{6}$$

where U = flow speed (m/s); the subscripts of U represents the room location in a matrix form, for example, ${}_{i,j}U_{i,j+1}$ represents the speed of flow from Room (i, j) to Room $(i, j + 1)$; subscript 'e' represents the external space; q_H = reference velocity pressure (N/m^2); l = distance from the center of a Room to that of the next Room (or to the edge of the Room), parallel to the flow (m); ${}_eC$ = external pressure coefficient at the gap location; C = layer pressure coefficient; the subscripts of ${}_eC$ and C represent the Room location; C_L = shape resistance coefficient for the cavity flow in the x or y direction; C_{Le} = pressure loss coefficient of the gap (shape resistance coefficient) in the z direction, depending on the gap configuration; and Δp = pressure loss due to friction (N/m^2). When the boundary of a Room corresponds to the periphery of PV panel, the subscript should be replaced by 'e' in Equations (4) and (5). Note that Equations (4) and (5) are applied to the cavity flows under PV panels or to the gap flows at the periphery of the PV system, while Equation (6) is applied to the flows through the gaps between PV panels. Although the values of C_L and C_{Le} depend on the gap configuration in a strict sense, they are assumed to be 1.0 for simplicity. This assumption can be accepted, because the width of gaps and the depth of cavity are relatively large. However, a detailed examination, such as a test with full-scale specimens [50], is required for validation.

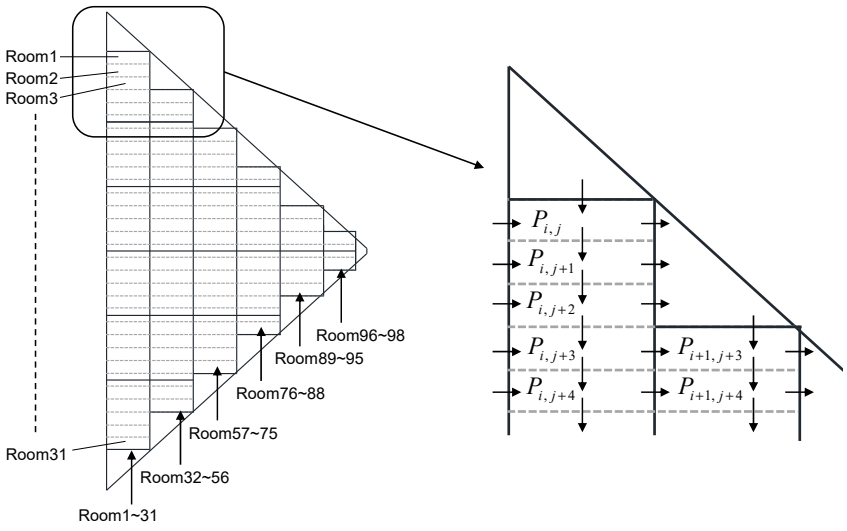

Figure 20. Definition of Rooms under PV panels.

The cavity flow under PV panels is assumed laminar [35,36]. The external pressure coefficients ${}_eC$ at the location of gaps in Equations (4)–(6) are obtained from the wind tunnel experiment mentioned in the previous section. Because the location of gaps does not coincide with that of pressure taps on the wind tunnel model, a spatial interpolation using the cubic spline function is applied to the experimental data; the value at the center of each gap is used as a representative value for the gap. Considering the calculation load, the above equations are solved by the 4th order Runge–Kutta method. Assuming the weak

compressibility of the air and an adiabatic condition, the internal pressure P in each Room (layer pressure) can be obtained by the following equation (see [49]):

$$\frac{dP}{dt} = \frac{\gamma P_0}{V_0} \sum_{m=1}^{M} Q_m \tag{7}$$

where γ = heat capacity ratio of the air; P_0 = atmospheric pressure (N/m^2); V_0 = volume of Room (m^3); Q_m = flow rate (m^3/s) at gap m; M = total number of gaps; and t = time (s). The layer pressure at the next time step is calculated by the Euler method with a time increment Δt of 1/8000 s. The sampling interval employed in the pressure measurements (Section 3) was approximately 0.036 s (=1/800 s $\times$ 29) at full scale, which is longer than Δt. Therefore, a temporal interpolation using the cubic spline function is applied to the time histories of wind pressure coefficients obtained from the wind tunnel experiment.

The wind force coefficient C_f of PV panel is provided by Equation (3) mentioned above. Here, the values of C_{pt} are obtained from the above-mentioned wind tunnel experiment, while those of C_{pl} are provided by the numerical simulation.

3.2. Comparison with the Experimental Results

Figure 21 shows comparisons between experiment and simulation for the distributions of mean layer pressure coefficients $\overline{C}_{pl}$ for Model B1 when $\theta = 0^\circ$, 45° and 90°. Note that the distribution on a quarter of the roof (shaded area of Figure 9) is depicted in the figure. Figure 22 compares the simulated results with the experimental ones for $\overline{C}_{pl}$ at each pressure tap when $\theta = 0^\circ$, 45° and 90°; the tap numbers are defined as shown in Figure 23. The agreement is generally good. When $\theta = 0^\circ$, the simulation results at Taps 2–6 located near the windward eaves are somewhat larger in magnitude than experimental ones; the largest difference is about 0.2. However, the absolute values of $\overline{C}_{pl}$ is relatively small at these pressure taps. A similar comparison is made for the minimum peak layer pressure coefficients $\check{C}_{pl}$ in Figure 24. When $\theta = 0^\circ$, the simulation results are somewhat larger in magnitude than the experimental ones; the largest difference is about 0.6. The difference is relatively large at pressure taps near the windward eaves, which may be due to a difference in the geometry of the roof's windward edge where the flow separation occurs. In the wind tunnel experiment, PV panels are installed on the roof, while the simulation uses the wind pressure data on the bare roof.

The simulation tends to overestimate the values of $\left|\overline{C}_{pl}\right|$ and $\left|\check{C}_{pl}\right|$ to some degree. When $\theta = 45^\circ$, the agreement is generally good except for Tap 20 located near the roof top, where the local pressure may be affected by the ridge configuration significantly. When $\theta = 90^\circ$, the simulation underestimates the magnitude of $\check{C}_{pl}$ at several pressure taps located near the eaves, such as Taps 3–5. This may be due to the effect of a difference in the eaves configuration. The result for Tap 20 is similar to that observed when $\theta = 45^\circ$. However, the simulation captures the largest wind force coefficient at Tap 1. The data plotted in Figure 24 are the results obtained by applying ensemble averaging to the results of 10 times of simulations. Figure 25 shows the standard deviation ($\sigma_{\check{C}_{pl}}$) of $\check{C}_{pl}$ obtained from these ten simulation data. Although the value of $\sigma_{\check{C}_{pl}}$ is generally small, we can see some cases where it is relatively large, for example, $\sigma_{\check{C}_{pl}} > 0.1$. In these cases the absolute value of $\overline{C}_{pl}$ is also large. Therefore, the coefficient of variation, defined by $\sigma_{\check{C}_{pl}} / \left|\hat{C}_{pl}\right|$, is smaller than 0.1 in most cases.

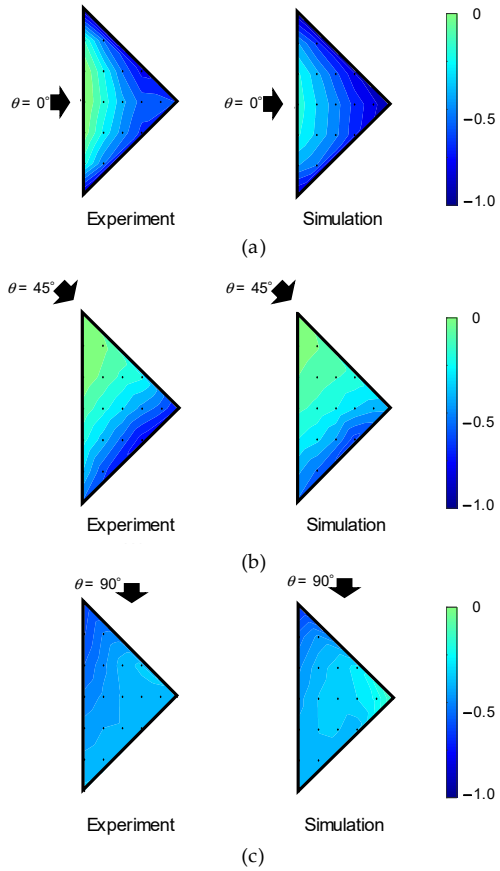

Figure 21. Comparison between simulation and experiment for the distributions of mean layer pressure coefficients (Model B1): (**a**) $\theta = 0°$; (**b**) $\theta = 45°$; (**c**) $\theta = 90°$.

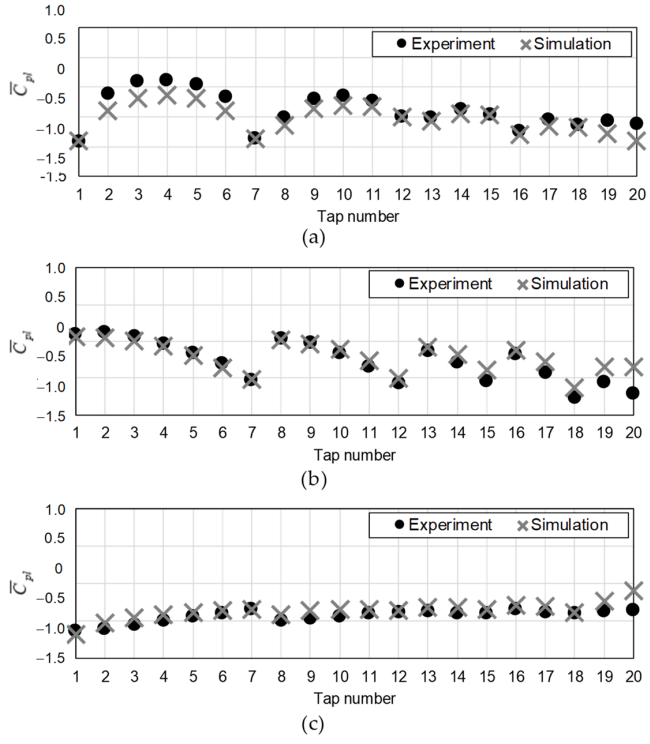

Figure 22. Comparison between simulation and experiment for the mean layer pressure coefficients (Model B1) at each pressure tap: (**a**) $\theta = 0°$; (**b**) $\theta = 45°$; (**c**) $\theta = 90°$.

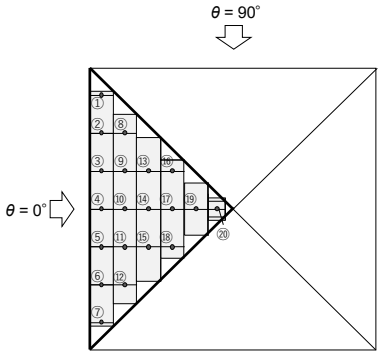

Figure 23. Definition of tap numbers.

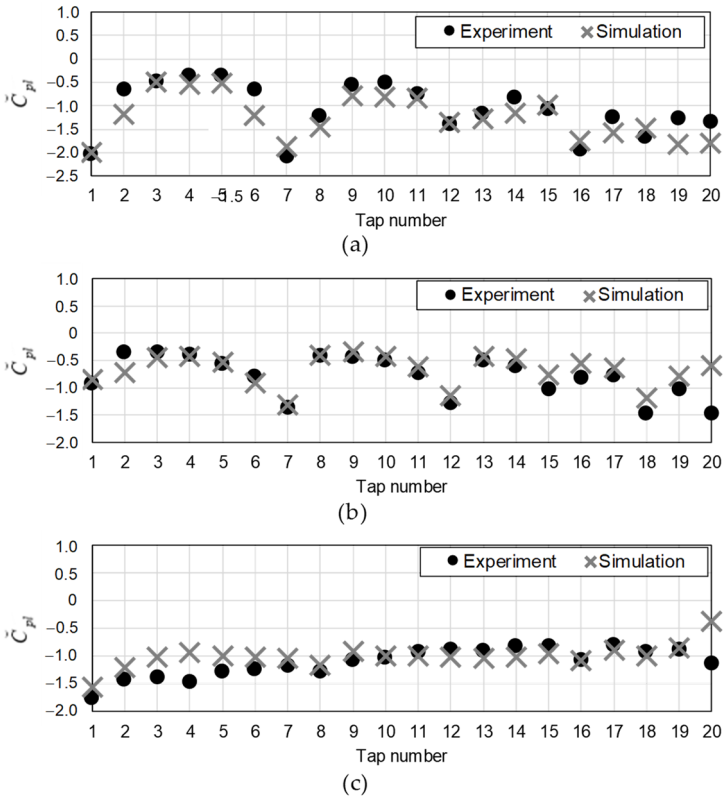

Figure 24. Comparison between simulation and experiment for the minimum peak layer pressure coefficients (Model B1) at each pressure tap: (**a**) $\theta = 0°$; (**b**) $\theta = 45°$; (**c**) $\theta = 90°$.

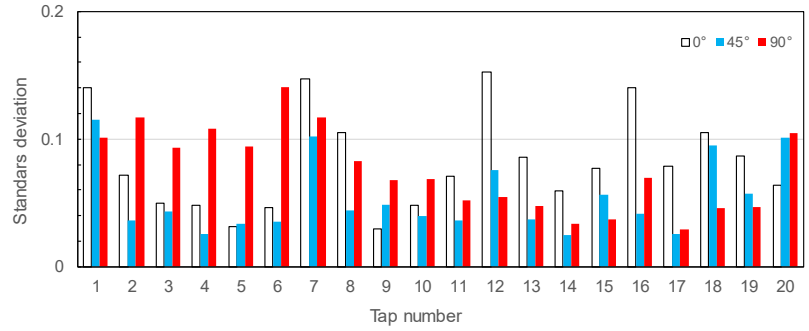

Figure 25. Standard deviation of the minimum peak layer pressure coefficient for $\theta = 0$, 45 and 90° (Model B1).

Considering that the thickness of PV panels and the distance between the lower surface of PV panels and the roof surface are both smaller in practical PV systems than in the wind tunnel model, the effect of roof configuration at the edges, whether PV panels are installed or not, on the layer pressures is expected to be smaller than those observed here. Therefore, it can be concluded that the numerical simulation employed in the present paper is used for estimating the layer pressures appropriately.

4. Concluding Remarks

The present paper investigates the wind loads on PV panels installed parallel to sloped roofs of residential houses, including the edge zones where large suctions are generated by flow separation. The main objective of the present paper is to investigate the application of a numerical simulation based on the unsteady Bernoulli equation to the estimation of pressures in the space under PV panels (called 'layer pressures', here), in which the time histories of external pressure coefficients on the bare roof (roof with no PV panel) is used. Because it is difficult to make a wind tunnel model of PV panels with the same geometric scale as that of the building, we focus on such a numerical simulation.

First, we made a wind tunnel experiment using three models of a square-roof building, named Models 'A', 'B0' and 'B1'. Model A had no PV panels installed on the roof. PV panels were installed on the roof with no gap between them for Model B0 and with a small gap between them for Model B1. In any case, PV panels located near the roof edges were subjected to large up-lift forces. The wind pressure distribution on the upper surface of PV panels was similar to that on the roof of Model A (bare roof). This means that installing PV panels on the roof does not affect the flow around the roof significantly. This also implies that we can estimate the layer pressures for Models B0 and B1 from the external pressure coefficients on Model A. This finding is very important from a practical viewpoint. Indeed, various arrangements of PV panels are used. Once we have measured the wind pressures on the bare roof, we can apply the same data to the simulation of layer pressures for any arrangement of PV panels. A comparison for the wind force coefficients on PV panels between Models B0 and B1 indicated that the magnitude of wind force coefficients for Model B1 was somewhat smaller in magnitude than that for Model B0. This feature may be due to the effect of pressure equalization caused by gaps between PV panels, which were represented by small circular holes in the present wind tunnel model. The negative wind forces (up-lift forces), which generally dictate the structural design of PV panels, can be estimated on the safer side from the wind pressures on the roof of Model A (bare roof), assuming that the wind pressures on the upper surface of PV panels are the same as those on the bare roof and the wind pressure on the lower surface of PV panel is zero.

Then, we applied a numerical simulation based on the unsteady Bernoulli equation to the estimation of layer pressures. The layer pressure coefficients are estimated from the time histories of external pressures on Model A at the location of gaps. The simulation results for the layer pressure coefficients on Model B1 were compared with the experimental ones. A relatively good agreement between them was observed. The maximum difference in the minimum peak layer pressure coefficient was about 0.5. This result implies that the numerical simulation employed in the present study is useful for estimating the wind loads on PV panels installed parallel to sloped roofs.

The present simulation model is based on the unsteady Bernoulli equation and the time histories of external pressure coefficients measured on the bare roof in a wind tunnel. Therefore, it cannot be applied to a case where the assumptions employed in the present model are not satisfied, for example, when the gap between PV panels and the distance between the lower surface of PV panels and the roof are so large that the flow speeds in the gaps and cavity are high. Furthermore, it cannot be applied to a case where the installation of PV panels on the roof affects the flow around the roof significantly, for example, when the height of PV panels is so high that the wind blows into the space between PV panels and roof. In such cases, a CFD simulation using ELS (Large Eddy Simulation) may be useful; however, it requires very fine mesh and high-spec computer for obtaining accurate

solutions. It was found that the gap between PV panels might reduce the net wind forces on PV panels significantly due to the effect of pressure equalization. The optimum size from the viewpoint of wind load reduction can be obtained from a series of simulations, in which the gap size is changed over a wide range. This is the subject of our future study; a preliminary study has been carried out by Yambe et al. [51].

Author Contributions: Conceptualization, Y.U.; Data curation, T.Y.; Formal analysis, T.Y.; Investigation, Y.U., T.Y. and A.Y.; Methodology, Y.U., T.Y. and A.Y.; Project administration, Y.U.; Software, T.Y.; Supervision, Y.U.; Validation, T.Y.; Writing—review & editing, Y.U. All authors have read and agreed to the published version of the manuscript.

Funding: This research received no external funding.

Informed Consent Statement: Not applicable.

Conflicts of Interest: The authors declare no conflict of interest.

References

1. Japan Association for Wind Engineering, Tokyo Polytechnic University. *Manual of Wind Resistant Design for Photovoltaic System*; Japan Association for Wind Engineering: Tokyo, Japan, 2017. (In Japanese)
2. Aly, A.M.; Bitsuamlak, G. Aerodynamics of ground-mounted solar panels: Test model scale effects. *J. Wind. Eng. Ind. Aerodyn.* **2013**, *123*, 250–260. [CrossRef]
3. Strobel, K.; Banks, D. Effects of vortex shedding in arrays of long inclined flat plates and ramifications for ground-mounted photovoltaic arrays. *J. Wind. Eng. Ind. Aerodyn.* **2014**, *133*, 146–149. [CrossRef]
4. Jubayer, C.M.; Hangan, H. Numerical simulation of wind effects on a stand-alone ground mounted photovoltaic (PV) system. *J. Wind. Eng. Ind. Aerodyn.* **2014**, *134*, 56–64. [CrossRef]
5. Jubayer, C.M.; Hangan, H. A numerical approach to the investigation of wind loading on an array of ground mounted solar photovoltaic (PV) panels. *J. Wind. Eng. Ind. Aerodyn.* **2016**, *153*, 60–70. [CrossRef]
6. Ginger, J.D.; Bodhinayake, G.G.; Ingham, S. Wind loads for designing ground-mounted solar-panel arrays. *Aust. J. Struct. Eng.* **2019**, *20*, 204–218. [CrossRef]
7. Browne, M.T.L.; Taylor, Z.J.; Li, S.; Gamble, S. A wind load design method for ground-mounted multi-row solar arrays based on a compilation of wind tunnel experiments. *J. Wind. Eng. Ind. Aerodyn.* **2020**, *205*, 104. [CrossRef]
8. Yemenici, O.; Aksoy, M.O. An experimental and numerical study of wind effects on a ground-mounted solar panel at different panel tilt angles and wind directions. *J. Wind. Eng. Ind. Aerodyn.* **2021**, *213*, 104630. [CrossRef]
9. Güemes, A.; Fajardo, P.; Raiola, M. Experimental assessment of RANS models for wind load estimation over solar-panel arrays. *Appl. Sci.* **2021**, *11*, 2496. [CrossRef]
10. Wood, G.S.; Denoon, R.O.; Kwok, K.C.S. Wind loads on industrial solar panel arrays and supporting roof structure. *Wind. Struct.* **2001**, *4*, 481–494. [CrossRef]
11. Kopp, G.A.; Farquhar, S.; Morrison, M.J. Aerodynamic mechanisms for wind loads on tilted, roof-mounted, solar arrays. *J. Wind. Eng. Ind. Aerodyn.* **2012**, *111*, 40–52. [CrossRef]
12. Kopp, G.A.; Banks, D. Use of the wind tunnel test method for obtaining design wind loads on roof-mounted solar arrays. *J. Struct. Eng. ASCE* **2013**, *139*, 284–287. [CrossRef]
13. Banks, D. The role of corner vortices in dictating peak wind loads on tilted flat solar panels mounted on large, flat roofs. *J. Wind. Eng. Ind. Aerodyn.* **2013**, *123*, 192–201. [CrossRef]
14. Browne, M.T.L.; Gibbons, M.P.M.; Gamble, S.; Galsworthy, J. Wind loading on tilted roof-top solar arrays: The parapet effect. *J. Wind. Eng. Ind. Aerodyn.* **2013**, *123*, 202–213. [CrossRef]
15. Cao, J.; Yoshida, A.; Saha, P.K.; Tamura, Y. Wind loading characteristics of solar arrays mounted on flat roofs. *J. Wind. Eng. Ind. Aerodyn.* **2013**, *123*, 214–225. [CrossRef]
16. Kopp, G.A. Wind loads on low-profile, tilted, solar arrays placed on large, flat, low-rise building roofs. *J. Struct. Eng. ASCE* **2014**, *140*, 04013057. [CrossRef]
17. Stathopoulos, T.; Zisis, I.; Xypnitou, E. Local and overall wind pressure and force coefficients for solar panels. *J. Wind. Eng. Ind. Aerodyn.* **2014**, *125*, 195–206. [CrossRef]
18. Wang, J.; Yang, Q.; Tamura, Y. Effects of building parameters on wind loads on flat-roof-mounted solar arrays. *J. Wind. Eng. Ind. Aerodyn.* **2018**, *174*, 210–224. [CrossRef]
19. Wang, J.; Phuc, P.V.; Yang, Q.; Tamura, Y. LES study of wind pressure and flow characteristics of flat-roof-mounted solar arrays. *J. Wind. Eng. Ind. Aerodyn.* **2020**, *198*, 104096. [CrossRef]
20. Wang, J.; Yang, Q.; Phuc, P.V.; Tamura, Y. Characteristics of conical vortices and their effects on wind pressures on flat-roof-mounted solar arrays by LES. *J. Wind. Eng. Ind. Aerodyn.* **2020**, *200*, 104146. [CrossRef]

21. Alrawashdeh, H.; Stathopoulos, T. Wind loads on solar panels mounted on flat roofs: Effect of geometric scale. *J. Wind. Eng. Ind. Aerodyn.* **2020**, *206*, 104339. [CrossRef]
22. Geurts, C.; Blackmore, P. Wind loads on stand-off photovoltaic systems on pitched roofs. *J. Wind. Eng. Ind. Aerodyn.* **2013**, *123*, 239–249. [CrossRef]
23. Aly, A.M.; Bitsuamlak, G.T. Wind-induced pressures on solar panels mounted on residential homes. *J. Archit. Eng. ASCE* **2014**, *20*, 04013003. [CrossRef]
24. Stenabaugh, S.E.; Iida, Y.; Kopp, G.A.; Karava, P. Wind loads on photovoltaic arrays mounted parallel to sloped roofs on low-rise buildings. *J. Wind. Eng. Ind. Aerodyn.* **2015**, *139*, 16–26. [CrossRef]
25. Naeiji, A.; Raji, F.; Zisis, I. Wind loads on residential scale rooftop photovoltaic panels. *J. Wind. Eng. Ind. Aerodyn.* **2017**, *168*, 228–246. [CrossRef]
26. Takamori, K.; Nakagawa, N.; Yamamoto, M.; Okuda, Y.; Taniguchi, T.; Nakamura, O. Study on design wind force coefficients for photovoltaic modules installed on low-rise building. *AIJ J. Technol. Des.* **2015**, *21*, 67–70. (In Japanese) [CrossRef]
27. *JIS C 8955:2017*; Japanese Industrial Standard. Load Design Guide on Structures for Photovoltaic Array. Japanese Standards Association: Tokyo, Japan, 2017.
28. Uematsu, Y.; Isyumov, N. Review Wind pressures acting on low-rise buildings. *J. Wind. Eng. Ind. Aerodyn.* **1999**, *82*, 1–25. [CrossRef]
29. Uematsu, Y. Peak gust pressures acting on low-rise building roofs. In Proceedings of the Eighth East Asia-Pacific Conference on Structural Engineering and Construction 2001, Singapore, 5–7 December 2001.
30. Amano, T.; Fujii, K.; Tazaki, S. Wind loads on permeable roof-blocks in roof insulation systems. *J. Wind. Eng. Ind. Aerodyn.* **1988**, *29*, 39–48. [CrossRef]
31. Okada, H.; Ohkuma, T.; Katagiri, J. Study on estimation of wind pressure under roof tiles. *J. Struct. Constr. Eng. Archit. Inst. Jpn.* **2008**, *73*, 1943–1950. (In Japanese) [CrossRef]
32. Oh, J.H.; Kopp, G.A. Modeling of spatially and temporary-varying cavity pressures in air-permeable, double-layer roof systems. *Build. Environ.* **2014**, *82*, 135–150. [CrossRef]
33. Uematsu, Y.; Shimizu, Y.; Miyake, Y.; Kanegae, Y. Wind-induced scattering of permeable unit flooring decks loosely laid on rooftops and balconies of high-rise buildings. *Tech. Trans. Civ. Eng.* **2015**, *2-B*, 191–213.
34. Watanabe, K.; Uematsu, Y. Evaluation of wind loads on ventilated exterior wall systems. *J. Wind. Eng. Jpn. Assoc. Wind. Eng.* **2019**, *44*, 23–32. (In Japanese) [CrossRef]
35. Oh, J.H.; Kopp, G.A. An experimental study of pressure equalization on double-layered roof system of low-rise buildings. In Proceedings of the 6th International Conference on Computational Wind Engineering, Hamburg, Germany, 8–12 June 2014.
36. Oh, J.H.; Kopp, G.A.; Inculet, D.R. The UWO contribution to the NIST aerodynamic database for wind loads on low buildings: Part 3. Internal pressures. *J. Wind. Eng. Ind. Aerodyn.* **2007**, *95*, 755–779. [CrossRef]
37. Architectural Institute of Japan. *Recommendations for Loads on Buildings*; Architectural Institute of Japan: Tokyo, Japan, 2015.
38. Tieleman, H.W.; Reinhold, T.A.; Marshall, R.D. On the wind-tunnel simulation of the atmospheric surface layer for the study of wind loads on low-rise buildings. *J. Wind. Eng. Ind. Aerodyn.* **1978**, *3*, 21–38. [CrossRef]
39. Tieleman, H.W. Pressures on surface-mounted prisms: The effects of incident turbulence. *J. Wind. Eng. Ind. Aerodyn.* **1993**, *49*, 289–299. [CrossRef]
40. Tieleman, H.W.; Hajj, M.R.; Reinhold, T.A. Wind tunnel simulation requirements to assess wind loads on low-rise buildings. *J. Wind. Eng. Ind. Aerodyn.* **1998**, *74–76*, 675–686. [CrossRef]
41. *ASCE/SEI 49-12*; Wind Tunnel Testing for Buildings and Other Structures. American Society of Civil Engineers: Reston, VA, USA, 2012.
42. Meecham, D.; Surry, D.; Davenport, A.G. The magnitude and distribution of wind-induced pressures on hip and gable roofs. *J. Wind. Eng. Ind. Aerodyn.* **1991**, *38*, 257–272. [CrossRef]
43. Xu, Y.L.; Reardon, G.F. Variations of wind pressure on hip roofs with roof pitch. *J. Wind. Eng. Ind. Aerodyn.* **1998**, *73*, 267–284. [CrossRef]
44. Ahmad, S.; Kumar, K. Effect of geometry on wind pressures on low-rise hip roof buildings. *J. Wind. Eng. Ind. Aerodyn.* **2002**, *90*, 755–779. [CrossRef]
45. Ahmad, S.; Kumar, K. Wind pressures on low-rise hip roof buildings. *Wind. Struct.* **2002**, *5*, 493–514. [CrossRef]
46. Takamori, K.; Nishimura, H.; Asami, R.; Somekawa, D.; Aihara, T. Wind pressures on hip roofs of a low-rise building–Case of square plan. In Proceedings of the 20th National Symposium on Wind Engineering 2008, Tokyo, Japan, 3–5 December 2008; pp. 463–466. (In Japanese).
47. Aihara, T.; Asami, Y.; Nishimura, H.; Takamori, K.; Asami, R.; Somekawa, D. An area correct factor for the wind pressure coefficient for cladding of hip roof–The case of square plan hip roof with roof pitch of 20 degrees. In Proceedings of the 20th National Symposium on Wind Engineering 2008, Tokyo, Japan, 3–5 December 2008; pp. 463–466. (In Japanese).
48. Shao, S.; Tian, Y.; Yang, Q.; Stathopoulos, T. Wind-induced cladding and structural loads on low-rise buildings with 4:12-splped hip roofs. *J. Wind. Eng. Ind. Aerodyn.* **2019**, *193*, 103948. [CrossRef]
49. Uematsu, Y.; Yambe, T.; Watanabe, T.; Ikeda, H. The benefit of horizontal photovoltaic panels in reducing wind loads on a membrane roofing system on a flat roof. *Wind* **2020**, *1*, 44–62. [CrossRef]

50. Yambe, T.; Uematsu, Y.; Sato, K.; Watanabe, T. Wind loads on photovoltaic systems installed parallel to the roof of flat-roofed building and its wind load reduction effect on the roofing system. *AIJ J. Technol. Des.* **2020**, *26*, 461–466. (In Japanese) [CrossRef]
51. Yambe, T.; Yamamoto, A.; Uematsu, Y. Wind loads of photovoltaic panels mounted on a hip roof to the edge and their wind-load reduction effect on roof cladding. *J. Struct. Constr. Eng. Archit. Inst. Jpn.* **2021**, *86*, 1581–1588. (In Japanese) [CrossRef]